analytical chemistry

pubs.acs.org/ac Article

Peptide-Based Biosensor with a Luminescent Copper-Based Metal–Organic Framework as an Electrochemiluminescence Emitter for Trypsin Assay

Xianzhen Song, Lu Zhao, Chuannan Luo, Xiang Ren, Lei Yang,* and Qin Wei*

Cite This: *Anal. Chem.* 2021, 93, 9704–9710 Read Online

ACCESS | Metrics & More | Article Recommendations | Supporting Information

ABSTRACT: A copper-based metal–organic framework (JUC-1000) has emerged as a promising electrochemiluminescence (ECL) emitter in the domains of bioanalysis and immunoassay. Herein, a highly efficient signal "on–off" peptide-based biosensor was constructed for trypsin (TPN) assay. JUC-1000 synthesized using an organic ligand of H_4BDPO was functionalized as the ECL emitter, whose cathodic ECL behavior in aqueous media was first investigated using potassium persulfate ($K_2S_2O_8$) as the coreactant. To further amplify the ECL signal, highly catalytic Ag@CeO_2 nanoparticles were fabricated as both a substrate and an coreaction accelerator, which can efficiently catalyze the reduction of $S_2O_8^{2-}$ to generate more sulfate anion radicals ($SO_4^{\bullet-}$) for ECL enhancement, thereby generating strong and stable ECL signals in a "signal on" state. The functionalized JUC-1000 emitter was connected to the Ag@CeO_2 sensing layer though a heptapeptide (HWRGWVC, HGC), and TPN as the target can specifically cleave the carboxyl side of arginine residues in HGC, leading to the release of emitters in a "signal off" state. Based on the efficient signal-switching, the biosensor exhibited linear ECL responses to the added TPN concentration, realizing sensitive detection of TPN in 10 fg/mL to 100 ng/mL with a limit of detection of 3.46 fg/mL. This work proposed an attractive orientation for the fundamental research of applying transition metal–organic frameworks as ECL emitters in bioanalysis and immunoassay.

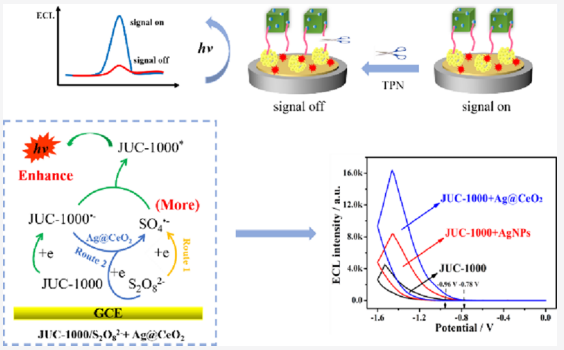

Recently, electrochemiluminescence (ECL) has been widely used in biological analysis, food safety, environmental monitoring, and other fields because of its high sensitivity, low toxicity, and fast analysis speed.[1−3] Because of their large specific surface area, unique porous structure, and excellent catalytic performance, metal–organic frameworks (MOFs) possess high adhibition prospects in many domains of catalysis, controlled drug release, and gas adsorption.[4−7] Until now, MOFs have made a rapid progress in reaction catalysis and luminophore loading for constructing ECL systems.[8,9] Nonetheless, there are few research reports on luminescent MOFs, which was mostly attributed to the fact that traditional organic ligands lack indispensable properties for ECL emission, such as redox activity and luminescence.[10,11] Hence, it is still challenging to develop MOFs with ECL properties.

A Cu^{2+}-based metal–organic framework (JUC-1000), a novel asymmetrical copper impeller in which copper atoms possess a unique pentacoordinate structure with four carboxylic acid groups, has excellent catalytic properties, acid and alkali resistance performance, and thermostability because of its open metal sites and unique functional groups.[4] In particular, the 1,3,5-triazine group contained in the JUC-1000 ligand provides a possibility for ECL emission.[12] Nevertheless, the application of JUC-1000 in ECL systems has not been covered so far. Herein, the cathodic ECL emission of JUC-1000 was first investigated using potassium persulfate ($K_2S_2O_8$) as the coreactant. Based on the strong and stable ECL signals in the aqueous phase, great application potential of JUC-1000 in ECL bioanalysis was observed.

To enhance the signal intensity of the biosensor for improving sensitivity, designing a ternary signal-amplification system containing a luminophore, a coreactant, and a coreaction accelerator is highly desirable. A properly matched coreaction accelerator for $K_2S_2O_8$ will significantly promote the production of sulfate anion ($SO_4^{\bullet-}$) radicals, thus improving the ECL reaction efficiency of JUC-1000 to obtain a dramatically amplified ECL intensity. Meanwhile, the introduction of an efficient coreaction accelerator could avoid the necessary demands of a high concentration of luminophores or coreactants in conventional ECL systems to achieve high sensitivity.[13,14] Considering this aspect, core–shell Ag@

Received: February 24, 2021
Accepted: June 28, 2021
Published: July 9, 2021

https://doi.org/10.1021/acs.analchem.1c00850
Anal. Chem. 2021, 93, 9704–9710

Scheme 1. Schematic Illustration of (a) Preparation of the JUC-1000-Fe_3O_4@Au-HGC Complex and (B) Construction Process of the Proposed Biosensor

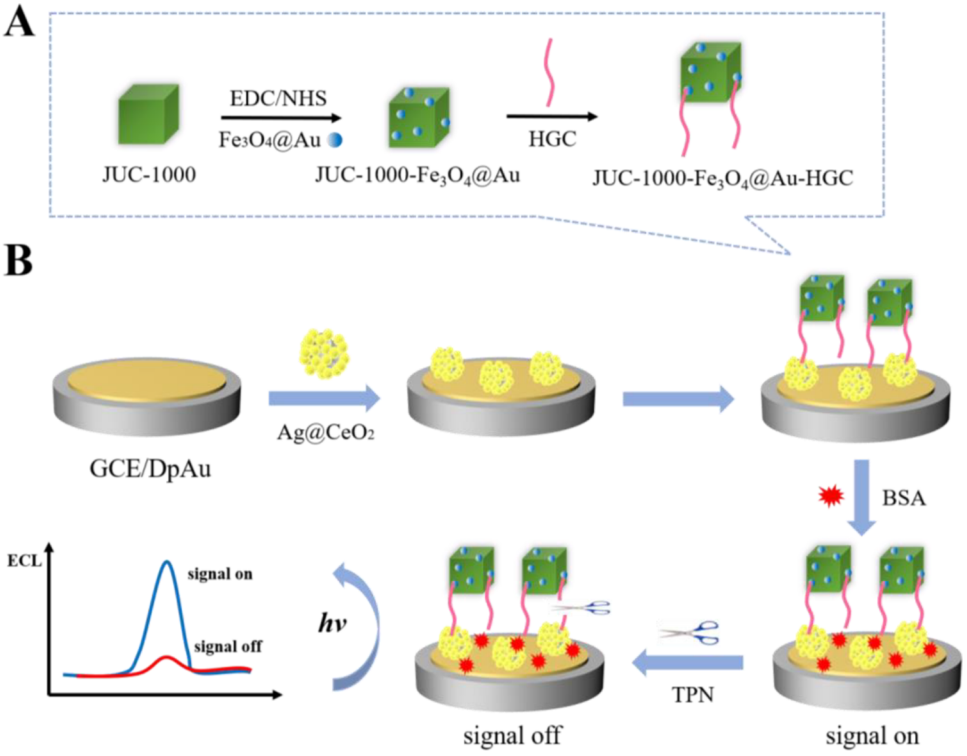

CeO_2 nanoparticles (NPs), with a unique cluster-like nanostructure where the highly catalytic Ag NPs were situated on the composite center and surrounded by CeO_2 NPs, were first employed as a coreaction accelerator.[15] The circumambient CeO_2 NPs can further improve catalytic activity by the fast reversible conversion of redox couple Ce^{4+}/Ce^{3+}.[16] Moreover, the formed Ag−CeO_2 interface in the core−shell composites can accelerate the electron transfer on the electrode surface, which can promote the production of $SO_4^{\bullet-}$. Hence, the ECL signal of the JUC-1000/$K_2S_2O_8$ system can be vastly enhanced by utilizing the core−shell Ag@CeO_2 NPs as an efficient coreaction accelerator.

Trypsin (TPN), an endonuclease, can specifically recognize and cleave the carboxyl side of arginine residues in the polypeptide chain, which is regarded as an important indicator for the identification of renal failure and pancreatic cancer.[17−20] As both a linker and specific cleavage site, a heptapeptide (HWRGWVC, HGC) with an arginine residue was introduced into the proposed ternary JUC-1000/$K_2S_2O_8$/Ag@CeO_2 system to develop a simple but reliable assay for TPN analysis. First, Ag@CeO_2 core−shell NPs were uniformly coated on the electrode surface as the sensing substrate, which can efficiently catalyze the reduction of $S_2O_8^{2-}$ to $SO_4^{\bullet-}$. Fe_3O_4@Au core−shell NPs were synthesized to connect with JUC-1000 through the condensation reaction between carboxyl and amino groups, which could not only accelerate electron transfer but also capture the HGC by the strong adsorption of Au NPs.[21] Conclusively, by modifying the JUC-1000-Fe_3O_4@Au-HGC bioconjugates on the Ag@CeO_2 substrate, a peptide-based biosensor was constructed in a "signal on" state. According to the TPN concentration (10 fg/mL−100 ng/mL), the HGC linker was specifically severed to release the JUC-1000-Fe_3O_4@Au into the solution, and the ECL signal was linearly reduced to a "signal off" state, obtaining a detection limit (LOD) of 3.46 fg/mL. As the very first ECL peptide biosensor that was ever constructed for TPN detection, it is believed that this work will provide both fundamental and crucial references for the clinical monitoring of TPN in renal failure and pancreatic cancer-related diseases.

EXPERIMENTAL SECTION

Preparation of the Cu^{2+}-MOF (JUC-1000). Before the preparation of JUC-1000, the organic ligand (H_4BDPO) was synthesized first. Briefly, 5-aminoisophthalic acid (1.81 g), NaOH (0.60 g), and $NaHCO_3$ (1.05 g) were dispersed in 60 mL of ultrapure water successively. After stirring at room temperature for 30 min, the cyanuric chloride (1.84 g) dissolved in 10 mL of 1,4-dioxane was added dropwise into the above solution. Next, the obtained mixed solution was stirred at natural temperature for 40 min and then continued stirring at 110 °C for 12 h. Ultimately, the solution was adjusted to pH = 2 via HCl (1 M) solution, and the obtained H_4BDPO was collected by filtration. After centrifugation (9000 rpm) and washing three times with ultrapure water, the final product was dried under vacuum at 60 °C.

For the preparation of JUC-1000, $Cu(NO_3)_2$ (0.2 g) and H_4BDPO (0.1 g) were dispersed into a mixture containing 60 mL of DMF, 5 mL of H_2O, and 2 mL of HNO_3, with stirring at natural temperature for 15 min. Posteriorly, the obtained mixture was heated at 90 °C for 3 days and then cooled to natural temperature. Finally, the blue crystalline product was acquired by centrifugation (9000 rpm) and washed twice with DMF and ultrapure water, respectively.

Preparation of the JUC-1000-Fe_3O_4@Au-HGC Complex. Primarily, the obtained JUC-1000 was dispersed in 2 mL of H_2O, and then 10 μL of a mixture composed of EDC (20

https://doi.org/10.1021/acs.analchem.1c00850
Anal. Chem. 2021, 93, 9704−9710

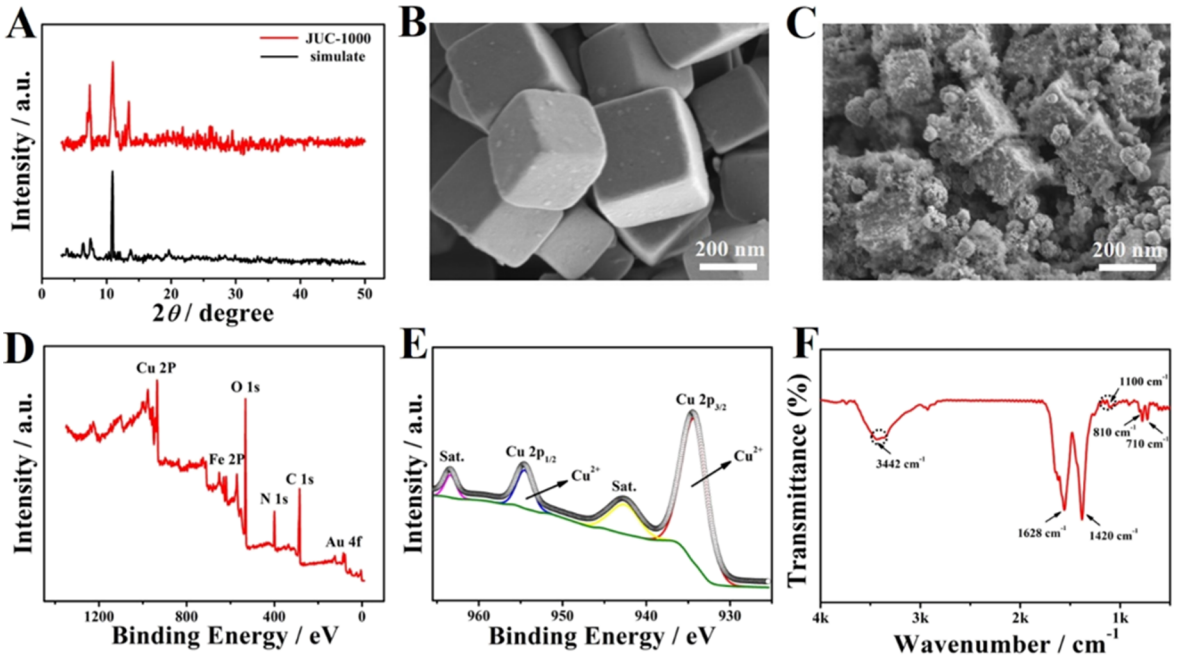

Figure 1. (A) Powder X-ray diffraction (XRD) pattern of JUC-1000. Scanning electron microscopy (SEM) images of (B) cubic JUC-1000 and (C) JUC-1000-Fe_3O_4@Au complex. X-ray photoelectron spectroscopy (XPS) spectra of (D) full region for JUC-1000-Fe_3O_4 @Au complex and (E) Cu 2p region. (F) Fourier transform infrared (FT-IR) spectrum of JUC-1000.

mM) and NHS (10 mM) was dropped into the above solution and shook at 4 °C for 2 h. Second, 5 mL of the prepared Fe_3O_4@Au solution was added into the above mixture to generate the JUC-1000-Fe_3O_4@Au complex via the condensation reaction between carboxyl and amino groups. Finally, HGC dispersed in 1 mL of phosphate buffer saline (PBS) was mixed with the above solution and hatched at 4 °C for 12 h. Hence, HGC could be easily attached to the surface of JUC-1000-Fe_3O_4@Au through Au-S bonding to obtain a JUC-1000-Fe_3O_4@Au-HGC complex.

Preparation of Core−Shell Ag@CeO_2 NPs. Ag@CeO_2 composites could be synthesized through a coprecipitation method.[22] Above all, $Ce(NO_3)_3{\cdot}6H_2O$ (1.01 g) and $AgNO_3$ (0.59 g) were dissolved in 10 mL of H_2O, and then the solution was added into 50 mL of diluted ammonia instantly. After stirring for 60 s, the mixture was transferred into an autoclave and reacted at 120 °C for 10 min. Conclusively, the coprecipitate was acquired through centrifugation (8000 rpm) and washed three times with ultrapure water and then calcined at 500 °C for 6 h.

Fabrication of the Peptide-Based Biosensor. The fabrication procedure is shown in Scheme 1. Primarily, a glassy carbon electrode (GCE) was polished to mirror via aluminum paste (0.3 and 0.05 μm), and then the processed GCE was soaked in $HAuCl_4$ (1%) solution at −0.2 V for 30 s, resulting in a layer of AuNPs. Afterward, 10 μL of Ag@CeO_2 and 12 μL of JUC-1000-Fe_3O_4@Au-HGC were dripped on the modified electrode in sequence, forming a sensing layer of JUC-1000-Fe_3O_4@Au-HGC/Ag@CeO_2/GCE. Ultimately, the obtained electrode was immersed in BSA (1%) for 2 h to block nonspecific sites. Importantly, each step needed to be flushed with ultrapure water to wipe off unconnected reagents during the fabrication procedure of the biosensor.

Measurement Procedure. For the detection of TPN, the as-prepared electrodes were immersed in disparate concentrations of TPN solution for 1 h and then washed with PBS (0.1 M). The ECL measurements were implemented through a three-electrode system containing a reference electrode, a platinum electrode, and a working electrode in 10 mL of PBS containing 80 mM $S_2O_8^{2-}$.

RESULTS AND DISCUSSION

Characterization of the JUC-1000-Fe_3O_4@Au Complex. The XRD patterns were studied to verify the successful preparation of JUC-1000. In Figure 1A, three evident characteristic peaks that were indexed to the cubic JUC-1000 (CCDC-1422688) were observed. Subsequently, the morphology and size of JUC-1000 and JUC-1000-Fe_3O_4@Au were characterized by SEM. JUC-1000 showed a unique cube construction with a side length of approximately 300 nm (Figure 1B). Meanwhile, Fe_3O_4@Au nanospheres were loaded on the surface of cubic JUC-1000 (Figure 1C), which indicated that the JUC-1000-Fe_3O_4@Au complex was synthesized successfully (the SEM mapping images are shown in Figure S3). Moreover, the XPS characterization was performed for elemental analysis of JUC-1000-Fe_3O_4@Au. As revealed in Figure 1D, all the characteristic peaks containing C 1 s, O 1 s, N 1 s, Cu 2p, Fe 2p, and Au 4f were present in JUC-1000-Fe_3O_4@Au. Meanwhile, the XPS spectrum of the Cu 2p region revealed four distinct characteristic peaks at 962.4, 953.6, 942.8, and 934.4 eV, respectively (Figure 1E). In detail, two peaks were associated with Cu $2p_{1/2}$ (953.6 eV) and Cu $2p_{3/2}$ (934.4 eV), and the other peaks could be seen as shake-up satellites, which foreboded that copper ions have a charge of plus two in JUC-1000.[23] Ultimately, the FT-IR spectra of JUC-1000 were obtained to further study its structure. In Figure 1F, there were several overt characteristic peaks at 3442, 1628, 1420, 1100, 810, and 710 cm^{-1}, respectively. To be specific, the two cuspidal and strong peaks at 1628 and 1420 cm^{-1} were ascribed to $\nu_{C=O}$ and ν_{C-O}, indicating the presence of carboxyl groups. The broad peak at 3442 cm^{-1} corresponded to ν_{O-H}, and a peak at 1100 cm^{-1} corresponded to ν_{C-N}, which referred

https://doi.org/10.1021/acs.analchem.1c00850
Anal. Chem. 2021, 93, 9704−9710

to the phenolic hydroxyl and triazinyl of JUC-1000, respectively. The other two characteristic peaks at 810 and 710 cm^{-1} ($\delta_{=C-H}$) revealed the position of substitution on the aromatic ring (1, 3, 5-ternary substitution).[24] In short, all the above results confirmed that JUC-1000-Fe_3O_4@Au was successfully prepared.

Characterization of Core−Shell Ag@CeO_2 Composites. In Figure 2A, the XRD patterns revealed two types of characteristic peaks, which were indexed to CeO_2 NPs (JCPDS 34-0394) and AgNPs (JCPDS 04−0783), respectively. As revealed in Figure 2B, Ag@CeO_2 NPs presented a typical state and were composed of several global NPs with an average diameter of approximate 40 nm. Meanwhile, HRTEM was employed to further study its microstructure. In Figure 2C, two lattice fringes were in good agreement with the (111) lattice plane of AgNPs and the (111) lattice plane of CeO_2 NPs, indicating that AgNPs were located in the center of the catalyst, which were surrounded by smaller CeO_2 NPs to form a unique core−shell structure. Figure 2D shows the EDS spectrum of Ag@CeO_2, and the founded elements, Ce, O, and Ag, proved the successful preparation of Ag@CeO_2 NPs.

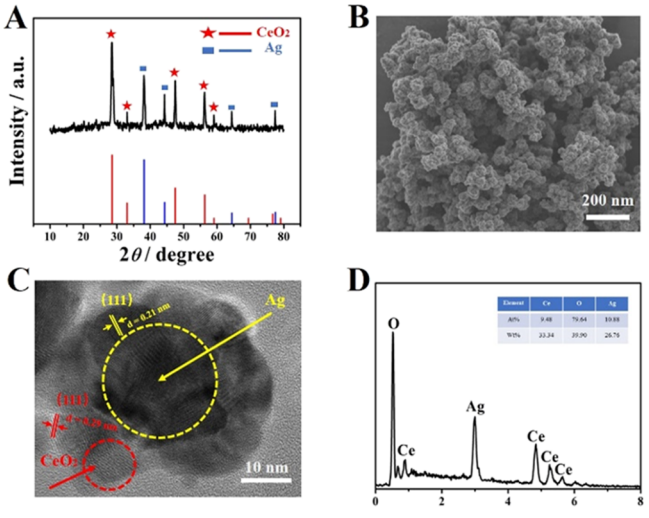

Figure 2. (A) XRD pattern, (B) SEM and (C) high-resolution transmission electron microscopy (HRTEM) images, and (D) energy-dispersive X-ray spectroscopy (EDS) spectrum of the core−shell Ag@CeO_2 NPs.

ECL Amplification of the JUC-1000/$S_2O_8^{2-}$/Ag@CeO_2 System. First, the ECL signals in different reaction systems were obtained to study a possible amplification mechanism. As revealed in Figure 3A, an extremely low ECL signal was obtained (1222 a.u., curve a), on account of an emission of singlet oxygen.[25] After modifying with JUC-1000, the ECL response was increased to 4528 a.u. (curve b), indicating that $K_2S_2O_8$ could serve as a coreactant of JUC-1000 to improve the ECL signal. Continuing to modify with Ag@CeO_2, the ECL intensity was approximately four times increased (curve c), revealing that Ag@CeO_2 could markedly enhance the ECL response in the JUC-1000/$K_2S_2O_8$ system. For further verifying this argument, the ECL responses of JUC-1000 and JUC-1000/Ag@CeO_2 in PBS were acquired. The results revealed that there was almost no difference between them (curves d and e), which convincingly proved that Ag@CeO_2 reacted with $S_2O_8^{2-}$ rather than JUC-1000.

To further elucidate the ECL amplification of the JUC-1000/$S_2O_8^{2-}$/Ag@CeO_2 system, the CV curves and ECL

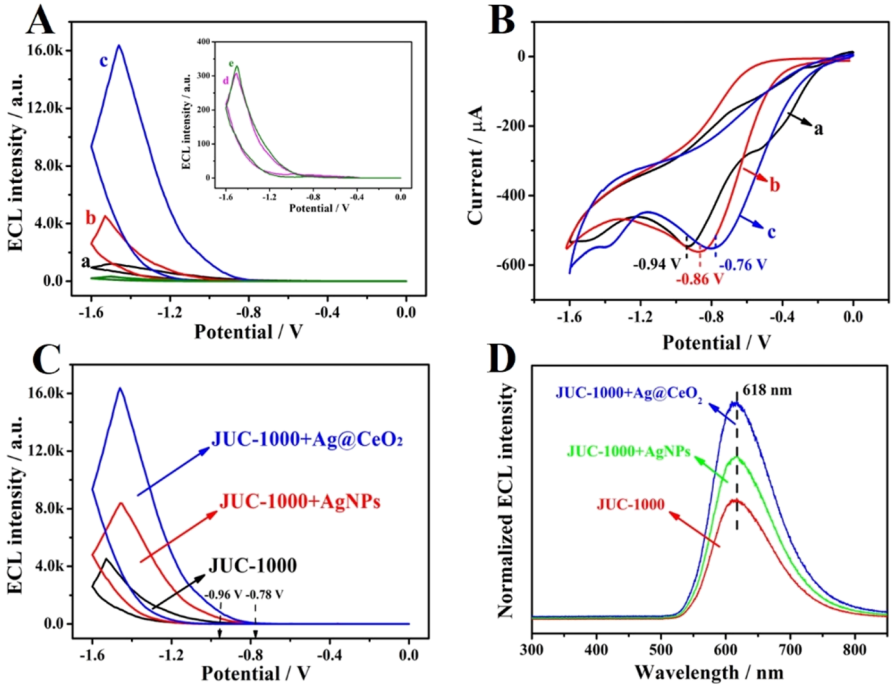

Figure 3. (A) ECL responses of (a) bare GCE, (b) JUC-1000- and (c) JUC-1000/Ag@CeO_2-modified electrodes 10 mL of PBS containing 80 mM $S_2O_8^{2-}$, and (e) JUC-1000- and (f) JUC-1000/Ag@CeO_2-modified electrodes in 10 mL of PBS without a coreactant. (B) Cyclic voltammetry (CV) curves and (C) ECL potential−intensity curves of (a) JUC-1000-, (b) JUC-1000/AgNP-, and (c) JUC-1000/Ag@CeO_2-modified electrodes in 10 mL of PBS containing 80 mM $S_2O_8^{2-}$, and (D) ECL spectra of (a) JUC-1000-, (b) JUC-1000/AgNP-, and (c) JUC-1000/Ag@CeO_2-modified electrodes in N_2-saturated PBS containing 80 mM $S_2O_8^{2-}$.

https://doi.org/10.1021/acs.analchem.1c00850
Anal. Chem. 2021, 93, 9704−9710

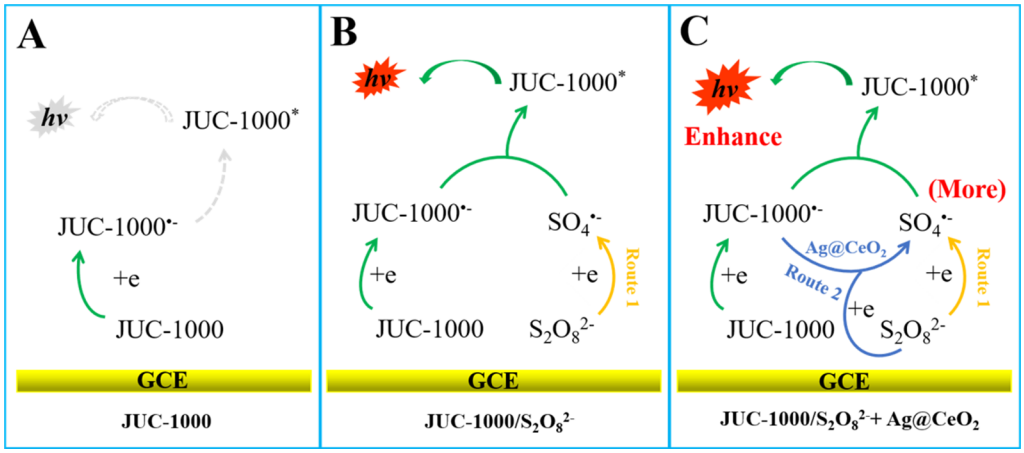

Figure 4. Possible luminescence mechanism of (A) JUC-1000, (B) JUC-1000/$S_2O_8^{2-}$, and (C) JUC-1000/$S_2O_8^{2-}$ + Ag@CeO_2 systems.

potential−intensity curves of JUC-1000, JUC-1000/AgNPs, and JUC-1000/Ag@CeO_2 were studied, respectively. As shown in Figure 3B, the JUC-1000-modified GCE revealed a maximum reduction peak of $S_2O_8^{2-}$ at −0.94 V (curve a).[26] After the further modification of AgNPs, the maximum reduction peak of $S_2O_8^{2-}$ was shifted to −0.86 V with an increased current intensity (curve b), indicating the splendid catalytic and conductive properties of AgNPs. When modifying the JUC-1000/GCE with Ag@CeO_2, the reduction peak of $S_2O_8^{2-}$ was further shifted to −0.76 V, thus highlighting the excellent catalytic activity of Ag@CeO_2 that can quickly reduce the $S_2O_8^{2-}$ into $SO_4^{\bullet-}$. Meanwhile, the corresponding ECL potential−intensity curves are presented in Figure 3C. Compared with JUC-1000- and JUC-1000/AgNP-modified electrodes, the ECL intensity of the JUC-1000/Ag@CeO_2/GCE was increased to about 16,000 a.u., and onset potential was shifted from −0.96 to −0.78 V, which verified the promoted ECL emission of JUC-1000 in the coreaction-accelerated reduction of $S_2O_8^{2-}$ by Ag@CeO_2 NPs.

Furthermore, the corresponding ECL spectra of JUC-1000-, JUC-1000/AgNP-, and JUC-1000/Ag@CeO_2-modified electrodes were acquired in N_2-saturated PBS containing 80 mM $S_2O_8^{2-}$. As shown in Figure 3D, JUC-1000 exhibited an emission peak at 618 nm. The ECL emission wavelength of JUC-1000/AgNP- and JUC-1000/Ag@CeO_2-modified electrodes was almost consistent with that of the JUC-1000/GCE, though the corresponding ECL signals were significantly improved compared to that of the JUC-1000/GCE. These results further demonstrated that Ag@CeO_2 had no direct reaction with the luminophore of JUC-1000 during the ECL emission process but could act as a robust coreaction accelerator to enhance the emission intensity indirectly.

Discussion of the Possible ECL Mechanism. The possible ECL mechanism of the JUC-1000/$S_2O_8^{2}$/Ag@CeO_2 system is shown in Figure 4. Primarily, JUC-1000 could not generate effective ECL emission because of the shortage of coreactants (Figure 4A). After $S_2O_8^{2-}$ was introduced as the coreactant, a small quantity of $SO_4^{\bullet-}$ was acquired with its reduction on the electrode surface and then reacted with JUC-1000$^{\bullet-}$ to generate an ECL signal (Figure 4B). Nevertheless, the ECL signal was greatly enhanced with the addition of Ag@CeO_2 NPs because of their efficient catalytic activity for the reduction of $S_2O_8^{2-}$ into plentiful $SO_4^{\bullet-}$ radicals (Figure 4C). To sum up, a possible reaction mechanism could be described as follows (eqs 123456). In route 1, $S_2O_8^{2-}$ was reduced to $SO_4^{\bullet-}$ on the electrode surface (eq 1). Based on the yielded amounts of $SO_4^{\bullet-}$ radicals, route 2 participated in the ECL emission process in which the fantastic Ce^{3+}/Ce^{4+} couple was involved in the reduction of $S_2O_8^{2-}$, and thus more $SO_4^{\bullet-}$ was produced through this triggered facile reaction between $S_2O_8^{2-}$ and Ce^{3+} (eqs 2 and 3). For the ECL emission procedure, JUC-1000 was electrochemically reduced to JUC-1000$^{\bullet-}$ on the electrode surface. Afterward, the produced reductive JUC-1000$^{\bullet-}$ would react with the oxidative $SO_4^{\bullet-}$ radicals to yield excited-state species JUC-1000*, thereby realizing a noteworthy ECL emission (eqs 456).

Route 1:

$$S_2O_8^{2-} + e^- \rightarrow SO_4^{2-} + SO_4^{\bullet-} \quad (1)$$

Route 2:

$$Ce^{4+} + e^- \rightarrow Ce^{3+} \quad (2)$$

$$Ce^{3+} + S_2O_8^{2-} \rightarrow Ce^{4+} + SO_4^{2-} + SO_4^{\bullet-} \quad (3)$$

ECL emission:

$$JUC - 1000 + e^- \rightarrow JUC - 1000^{\bullet-} \quad (4)$$

$$JUC - 1000^{\bullet-} + SO_4^{\bullet-} \rightarrow JUC - 1000^{*} + SO_4^{2-} \quad (5)$$

$$JUC - 1000^{*} \rightarrow JUC - 1000 + h\nu \quad (6)$$

Calibration Curve for TPN Assay. As displayed in Figure 5A, the ECL intensity was linearly decreased when the TPN concentrations increased from 10 fg/mL to 100 ng/mL.

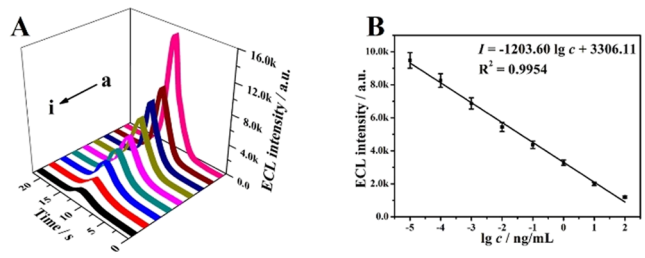

Figure 5. (A) ECL responses of the proposed biosensor for disparate TPN concentrations in 10 mL of PBS containing 80 mM $S_2O_8^{2-}$: (a) 0, (b) 10 fg/mL, (c) 100 fg/mL, (d) 1 pg/mL, (e) 10 pg/mL, (f) 100 pg/mL, (g) 1 ng/mL, (h) 10 ng/mL, and (i) 100 ng/mL. (B) Corresponding calibration curve for TPN detection.

https://doi.org/10.1021/acs.analchem.1c00850
Anal. Chem. 2021, 93, 9704−9710

Meanwhile, a linear equation was expressed as $I_{ECL} = -1203.60 \lg c + 3306.11$, with a correlation coefficient of 0.9954 (Figure 5B). In addition, a linear response range (10 fg/mL−100 ng/mL) and a LOD of 3.46 fg/mL were acquired through the calibration curve of ECL responses, which were better than those of other detection methods (Table 1). Hence, the peptide-based biosensor demonstrated an efficient and sensitive means for TPN testing.

Table 1. Comparison of ECL Analysis Means with Other Testing Platforms for TPN Testing

methods	linear range (ng/mL)	LOD (ng/mL)	references
SERS	0.1−1.0 × 10^4	0.1	27
colorimetry	2.5−200	2	28
electrochemistry	5−150	1.8	29
square wave voltammetry	100−1.00 × 10^6	10	30
fluorimetry	0.01−0.1	0.044	31
photoelectrochemical	0.1−1 × 10^6	0.032	20
ECL	1.00 × 10^{-5}-100	3.46 × 10^{-6}	this work

Specificity, Stability, and Repeatability of the Biosensor. It is widely known that specificity is a crucial index to evaluate the biosensor performance. In this study, prostate-specific antigen, amyloid-β protein, procalcitonin, carcinoembryonic antigen, glucose, ascorbic acid, alanine, and glutamine were used as the interferents to verify the specificity of the biosensor. In Figure 6A, the ECL responses of

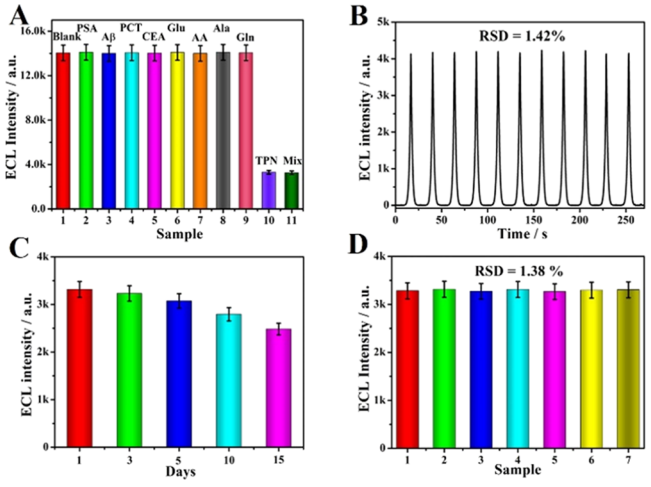

Figure 6. (A) Specificity, (B) operation (11 scans) and (C) storage (15 days) stability, and (D) repeatability of the proposed biosensor.

the interferents (10 ng/mL) had inappreciable variation compared with the blank sample. Furthermore, the biosensor incubated with the mixture (1 ng/mL of TPN and 10 ng/mL interferents) revealed a similar ECL signal to that of pure TPN (1 ng/mL), which suggested a good specificity of the biosensor.

To investigate the operation stability of the biosensor, the ECL responses of TPN under 11 cycles of consecutive potential scanning were obtained. In Figure 6B, the proposed biosensor exhibited good operation stability for TPN detection (relative standard deviation (RSD) = 1.31%). Meanwhile, the proposed biosensor revealed a good storage stability via following up the ECL response in long-term storage at 4 °C (Figure 6C). Additionally, the repeatability as another important factor of the biosensor performance evaluation was investigated through the ECL measurements of seven different electrodes. The results (RSD = 1.38%) in Figure 6D showed the good repeatability of the biosensor.

Real Sample Analysis of TPN. To study the feasibility of the biosensor in real sample analysis, the standard addition method was adopted by adding different concentrations of standard TPN samples into human serum for testing. Surprisingly, the results showed an admirable accuracy of the peptide-based biosensor with a recovery value ranging from 97.5 to 101%. Meanwhile, the RSD of the biosensor was from 2.2 to 2.7%, which foreboded that it had super detection precision (Table S1). Hence, the proposed biosensor exhibited great superiority for TPN detection in actual samples, indicating huge application potential in early diagnosis of pancreatic cancer.

CONCLUSIONS

In this work, the cathodic ECL behavior of a luminescent Cu-MOF (JUC-1000) was first investigated using $K_2S_2O_8$ as the coreactant in aqueous media. The sensing application of JUC-1000/$S_2O_8^{2-}$ was conducted by establishing a ternary sensing system for sensitive detection of TPN in which the Ag@CeO_2 NP formed layer was first utilized as an efficient coreaction accelerator that can efficiently catalyze the generation of oxidative $SO_4^{\bullet-}$ radicals for ECL enhancement. The JUC-1000-based emitter and the Ag@CeO_2 layer were connected by a polypeptide HGC, achieving a "signal on" state in the absence of TPN. After the addition of TPN, a noteworthy "signal off" state was achieved through the specific cleavage of arginine residues in HGC by TPN. Based on the "on−off" switching, the proposed biosensor performed sensitive and accurate concentration readout for real sample analysis of TPN. It is undeniable that this work will serve as a guide for the basic research of applying transition MOFs as ECL emitters in biosensing analysis.

ASSOCIATED CONTENT

Supporting Information

The Supporting Information is available free of charge at https://pubs.acs.org/doi/10.1021/acs.analchem.1c00850.

Cleavage site and structural formula of HGC, chemicals, and materials, apparatus, preparation of Fe_3O_4 nanospheres, preparation of Fe_3O_4@Au nanocomposites, advantages of the coprecipitation method, pretreatment of the serum samples, SEM images of Fe_3O_4 and Fe_3O_4@Au, SEM mapping images of JUC-1000-Fe_3O_4@Au, control experiments of oxygen removal, ECL time−intensity curve analysis, electrochemical behaviors of the proposed biosensor, optimization of experimental conditions, and actual sample analysis (PDF)

AUTHOR INFORMATION

Corresponding Authors

Lei Yang − *Collaborative Innovation Center for Green Chemical Manufacturing and Accurate Detection, Key Laboratory of Interfacial Reaction & Sensing Analysis in Universities of Shandong, School of Chemistry and Chemical Engineering, University of Jinan, Jinan, Shandong 250022, China;* orcid.org/0000-0003-2153-3570; Phone: +86

https://doi.org/10.1021/acs.analchem.1c00850
Anal. Chem. 2021, 93, 9704−9710

531 82765730; Email: yanglei_19940831@163.com; Fax: +86 531 82765969

Qin Wei − *Collaborative Innovation Center for Green Chemical Manufacturing and Accurate Detection, Key Laboratory of Interfacial Reaction & Sensing Analysis in Universities of Shandong, School of Chemistry and Chemical Engineering, University of Jinan, Jinan, Shandong 250022, China;* orcid.org/0000-0002-3034-8046; Phone: +86 531 82765730; Email: sdjndxwq@163.com; Fax: +86 531 82765969

Authors

Xianzhen Song − *Collaborative Innovation Center for Green Chemical Manufacturing and Accurate Detection, Key Laboratory of Interfacial Reaction & Sensing Analysis in Universities of Shandong, School of Chemistry and Chemical Engineering, University of Jinan, Jinan, Shandong 250022, China*

Lu Zhao − *Collaborative Innovation Center for Green Chemical Manufacturing and Accurate Detection, Key Laboratory of Interfacial Reaction & Sensing Analysis in Universities of Shandong, School of Chemistry and Chemical Engineering, University of Jinan, Jinan, Shandong 250022, China*

Chuannan Luo − *Collaborative Innovation Center for Green Chemical Manufacturing and Accurate Detection, Key Laboratory of Interfacial Reaction & Sensing Analysis in Universities of Shandong, School of Chemistry and Chemical Engineering, University of Jinan, Jinan, Shandong 250022, China*

Xiang Ren − *Collaborative Innovation Center for Green Chemical Manufacturing and Accurate Detection, Key Laboratory of Interfacial Reaction & Sensing Analysis in Universities of Shandong, School of Chemistry and Chemical Engineering, University of Jinan, Jinan, Shandong 250022, China;* orcid.org/0000-0002-4321-4282

Complete contact information is available at: https://pubs.acs.org/10.1021/acs.analchem.1c00850

Notes

The authors declare no competing financial interest.

■ ACKNOWLEDGMENTS

This study was supported by the National Key Scientific Instrument and Equipment Development Project of China (No. 21627809), the National Natural Science Foundation of China (Nos. 21777056 and 21427808), Special Foundation for Taishan Scholar Professorship of Shandong Province, Jinan Scientific Research Leader Workshop Project (2018GXRC024 and 2018GXRC021), and the Innovation Team Project of Colleges and Universities in Jinan (No. 2019GXRC027).

■ REFERENCES

(1) Hu, L. Z.; Xu, G. B. *Chem. Soc. Rev.* **2010**, *39*, 3275−3304.
(2) Xu, J. J.; Huang, P. Y.; Qin, Y.; Jiang, D. C.; Chen, H. Y. *Anal. Chem.* **2016**, *88*, 4609−4612.
(3) Yang, L.; Jia, Y.; Wu, D.; Zhang, Y.; Ju, H. X.; du, Y.; Ma, H. M.; Wei, Q. *Anal. Chem.* **2019**, *91*, 14066−14073.
(4) He, H. M.; Sun, Q.; Gao, W. Y.; Perman, J. A.; Sun, F. X.; Zhu, G. S.; Aguila, B.; Forrest, K.; Space, B.; Ma, S. Q. *Angew. Chem.* **2018**, *57*, 4657−4662.
(5) Wei, Y. S.; Zhang, M.; Zou, R. Q.; Xu, Q. *Chem. Rev.* **2020**, *120*, 12089−12174.
(6) Suresh, K.; Matzger, A. J. *Angew. Chem.* **2019**, *58*, 16790−16794.
(7) Zhao, L.; Kuang, X.; Kuang, R.; Tong, L.; Liu, Z. X.; Hou, Y.; Sun, X.; Wang, Z. L.; Wei, Q. *ACS Appl. Mater. Interfaces* **2020**, *12*, 1533−1538.
(8) Wang, S. S.; Zhao, Y. Y.; Wang, M. M.; Li, H. J.; Saqib, M.; Ge, C. H.; Zhang, X. D.; Jin, Y. D. *Anal. Chem.* **2019**, *91*, 3048−3054.
(9) Song, X. Z.; Shao, X. R.; Dai, L.; Fan, D. W.; Ren, X.; Sun, X.; Luo, C. N.; Wei, Q. *ACS Appl. Mater. Interfaces* **2020**, *12*, 9098−9106.
(10) Kent, C. A.; Liu, D.; Meyer, T. J.; Lin, W. B. *J. Am. Chem. Soc.* **2012**, *134*, 3991−3994.
(11) Wang, C.; Lin, W. B. *J. Am. Chem. Soc.* **2011**, *133*, 4232−4235.
(12) El-Sedik, M.; Almonasy, N.; Nepraś, M.; Bureš, F.; Dvořák, M.; Michl, M.; Čermák, J.; Hrdina, R. *Dyes Pigm.* **2012**, *92*, 1126−1131.
(13) Song, X. Z.; Li, X. J.; Wei, D.; Feng, R.; Yan, T.; Wang, Y. G.; Ren, X.; du, B.; Ma, H. M.; Wei, Q. *Biosens. Bioelectron.* **2019**, *126*, 222−229.
(14) Wu, F. F.; Zhou, Y.; Zhang, H.; Yuan, R.; Chai, Y. Q. *Anal. Chem.* **2018**, *90*, 2263−2270.
(15) Zhang, P.; Zhuo, Y.; Chang, Y. Y.; Yuan, R.; Chai, Y. Q. *Anal. Chem.* **2015**, *87*, 10385−10391.
(16) Wang, J. Y.; Zhuo, Y.; Zhou, Y.; Wang, H. J.; Yuan, R.; Chai, Y. Q. *ACS Appl. Mater. Interfaces* **2016**, *8*, 12968−12975.
(17) Dau, T.; Bartolomucci, G.; Rappsilber, J. *Anal. Chem.* **2020**, *92*, 9523−9527.
(18) Zhou, S.; Wang, L.; Chen, X. H.; Guan, X. Y. *ACS Sens.* **2016**, *1*, 607−613.
(19) Xu, S. M.; Zhang, F. M.; Xu, L. B.; Liu, X.; Ma, P. Y.; Sun, Y.; Wang, X. H.; Song, D. Q. *Sens. Actuators B: Chem.* **2018**, *273*, 1015−1021.
(20) Dai, H.; Chen, S. H.; Li, Y. L.; Zeng, B. S.; Zhang, S. P.; Hong, Z. S.; Lin, Y. Y. *Biosens. Bioelectron.* **2017**, *92*, 687−694.
(21) Li, Y. Z.; Li, T. T.; Chen, W.; Song, Y. Y. *ACS Appl. Mater. Interfaces* **2017**, *9*, 29881−29888.
(22) Yamazaki, K.; Kayama, T.; Dong, F.; Shinjoh, H. *J. Catal.* **2011**, *282*, 289−298.
(23) Zhao, L.; Kuang, X.; Chen, C.; Sun, X.; Wang, Z. L.; Wei, Q. *Chem. Commun.* **2019**, *55*, 10170−10173.
(24) Cai, Y. J.; Li, X. Y.; Wu, K. B.; Yang, X. F. *Anal. Chim. Acta* **2019**, *1062*, 78−86.
(25) Ma, M. N.; Zhuo, Y.; Yuan, R.; Chai, Y. Q. *Anal. Chem.* **2015**, *87*, 11389−11397.
(26) Dai, P. P.; Yu, T.; Shi, H. W.; Xu, J. J.; Chen, H. Y. *Anal. Chem.* **2015**, *87*, 12372−12379.
(27) Chen, L. X.; Fu, X. L.; Li, J. H. *Nanoscale* **2013**, *5*, 5905−5911.
(28) Miao, P.; Liu, T.; Li, X. X.; Ning, L. M.; Yin, J.; Han, K. *Biosens. Bioelectron.* **2013**, *49*, 20−24.
(29) Liang, R. P.; Tian, X. C.; Qiu, P.; Qiu, J. D. *Anal. Chem.* **2014**, *86*, 9256−9263.
(30) Stoytcheva, M.; Zlatev, R.; Cosnier, S.; Arredondo, M. *Electrochim. Acta* **2012**, *76*, 43−47.
(31) Liu, X.; Li, Y.; Jia, L.; Chen, S.; Shen, Y. H. *RSC Adv.* **2016**, *6*, 93551−93557.